On the Performance of IRS-Assisted Relay Systems

Diluka Loku Galappaththige, Alan Devkota, and Gayan Amarasuriya
School of Electrical, Computer, and Biomedical Engineering, Southern Illinois University, Carbondale, IL, USA 62901
Email: {diluka.lg, alan.devkota, gayan.baduge}@siu.edu

***Abstract*—This paper investigates the performance of intelligence reflective surface (IRS)-assisted relay systems. To this end, we quantify the optimal signal-to-noise ratio (SNR) attained by smartly controlling the phase-shifts of impinging electromagnetic waves upon an IRS. Thereby, a tightly approximated cumulative distribution function is derived to probabilistically characterize this optimal SNR. Then, we derive tight approximations/bounds for the achievable rate, outage probability, and average symbol error rate. Monte-Carlo simulations are used to validate our performance analysis. We present numerical results to reveal that the IRS-assisted relay system can boost the performance of end-to-end wireless transmissions.**

I. Introduction

An intelligence reflecting surface (IRS) having a large number of tiny passive reflectors can enable a controllable wireless propagation environment by introducing distinct delays to the reflected electromagnetic (EM) waves [1]–[4]. These delays in turn result in controllable phase-shifts, which can be used to intelligently reconfigure propagation properties of EM waves through the wireless medium. This feature of IRSs can be utilized to improve the signal-to-noise ratio (SNR) of an end-to-end communication between a transmitter and a receiver by enabling constructive additions of EM waves at a desired destination [5]. Due to the passive beamforming nature of the IRS, it enables energy efficient communication without actively generating additional EM signals from active radio-frequency chains/amplifiers [1]. Hence, IRSs have been recognized as one of the key enabling technologies for the next-generation wireless physical layer [1], [2].

Relay-assisted cooperative communications have been studied for well over two decades due to their potential of enhancing the performance of wireless systems [6]–[8]. Relaying can effectively reduce the end-to-end path-loss in terms of shorter-hop distances and amplify-and-forward (AF) or decode-and-forward (DF) operations at intermediate relays [6]–[8]. Relay-assisted system models can achieve broader coverage probability, improve spectral/energy efficiency, and enhance communication reliability.

Next, we summarize several important contributions to the development of IRS-assisted communication systems. References [1], [2] establish theoretical foundations of adopting IRSs for wireless communication by investigating practical realization and deployment aspects. In [5], IRSs are deployed in a distributed manner, and thereby, the corresponding performance bounds are evaluated for Nakagami-m fading. In [9], two computationally efficient algorithms based on alternative optimization techniques are proposed for transmit power allocation at the base station (BS) and reflective/passive beamforming at the IRS. In [10], a power consumption and energy efficiency comparison between IRSs and repetition-coded DF relaying is presented by considering ideal phase-shift adjustments in frequency-flat fading channels. Reference [11] analytically studies the differences and similarities between IRSs and relays. Thereby, it is shown that the relay-assisted systems can be outperformed by large RISs in terms of data rates. In [12], the performance of a single IRS-assisted wireless system is evaluated by deriving the outage probability, average symbol error rate (SER), diversity order, and ergodic capacity. These performance matrices are compared against an AF relay. In [13], a hybrid DF relay and IRS network is investigated, and thereby, a semi-definite relaxation technique based optimization scheme is proposed to design the reflecting coefficients at the IRS for maximizing the minimum achievable rate. In [14], the benefits of combining an IRS with a DF relay are studied.

Aforementioned all related prior research [1], [2], [5], [9]–[13] solely investigate either IRS-assisted communication systems or compare their performance with the relay-assisted counterparts. To the best of our knowledge, the fundamental performance metrics of the IRS-relay cascaded communication systems have not yet been investigated in the open literature. Thus, we aim to investigate the feasibility of employing an IRS-relay cascaded system for reaping the joint benefits of IRS and AF relays in a combined set-up. Thus, in our work, we develop an analytical framework to fill this important gap for deriving the performance bounds pertaining to an IRS-relay cascaded system. First, the end-to-end optimal SNR is characterized via probabilistic models by tightly approximating it by a mathematically tractable counterpart by invoking the central limit theorem (CLT). Thereby, a tight upper bound for the cumulative distribution function (CDF) of this approximated optimal SNR is derived. By using this CDF, tight bounds/approximations for the average achievable rate, SNR/rate outage probability, and average SER are derived in closed-form. Then, the tightness of our performance bounds/approximations is validated through Monte-Carlo simulations. Finally, a set of insightful numerical results is presented to explore the performance gains of the proposed IRS-assisted relay system.

Notation: A circularly symmetric Gaussian distributed random variable Y having μ_Y mean and σ_Y^2 variance is denoted by $Y \sim \mathcal{CN}\left(\mu_Y, \sigma_Y^2\right)$. The expectation and the variance of Y are denoted by $\mathbb{E}[Y]$ and $\mathbb{V}\mathrm{ar}[Y]$, respectively. The notation $\mathbf{y}^T$ denotes the transpose of the vector $\mathbf{y}$, and $C_n = \{0, 1, \cdots, n\}$.

II. System, channel and signal models

A. System and channel model

An IRS-assisted relay system is considered as shown in Fig. 1, in which a source (S) serves a destination (D) through a cascaded IRS-relay channel. The relay (R) is equipped with a single antenna, and it operates in half-duplex AF mode. The direct channels S-R and S-D are assumed to be unavailable due to severe blockage effects. The IRS consists of N passive

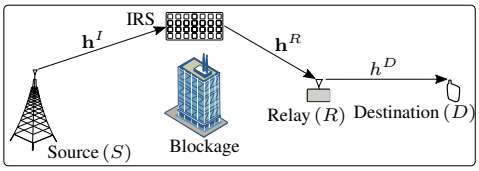

Fig. 1. System model-IRS-assisted relay network.

reflectors, and the phase-shifts of EM waves impinging on them can be intelligently controllable to ensure that the received signal at D can be constructively combined. For the sake of exposition, we use $\mathcal{N}\in\{1,\cdots,N\}$ to denote the set of passive reflectors at the IRS.

The channel coefficient between S and the nth reflector of the IRS is denoted by h_n^I, while h_n^R represents the channel between the nth reflector and R. Moreover, the channel between R and D is denoted by h^D. All of these channels can be modeled in polar-form as

$$u=\beta_u \mathrm{e}^{j\theta_u}, \tag{1}$$

where $u\in\{h_n^I,h_n^R,h^D\}$ and $n\in\mathcal{N}$. In (1), β_u denotes the envelop of u, and θ_u is the phase of u. Here, β_u is assumed to be independent Rayleigh distributed as [15]

$$f_{\beta_u}(x)=(x/\xi_u)\exp\left(-x^2/\left(2\xi_u\right)\right), \tag{2}$$

where $\xi_u=\zeta_u/2$ is the Rayleigh parameter, and ζ_u accounts for the large-scale fading/path-loss of the channel u. Since the IRS reflectors are co-located, we assume that large-scale fading parameters are the same for respective S-IRS and IRS-R channels.

B. Signal model

The signal transmitted by S reaches D through the IRS-R cascaded channel. To this end, we can express the signal received at R during the first time-slot as

$$y_R=\sqrt{P}(\mathbf{h}^R)^T\mathbf{\Theta}\mathbf{h}^I x+w_R, \tag{3}$$

where P denotes the transmit signal power at S, x is the signal intended for D satisfying $\mathbb{E}\left[|x|^2\right]=1$, and $w_R\sim\mathcal{CN}\left(0,\sigma_{w_R}^2\right)$ is an additive white Gaussian noise (AWGN) at R having zero mean and $\sigma_{w_R}^2$ variance. Furthermore, the channel vector between S and IRS is given by $\mathbf{h}^I=[h_1^I,\cdots,h_n^I,\cdots,h_N^I]^T\in\mathbb{C}^{N\times 1}$, and $(\mathbf{h}^R)^T=[h_1^R,\cdots,h_n^R,\cdots,h_N^R]\in\mathbb{C}^{1\times N}$ represents the channel vector between the IRS and R. In (3), $\mathbf{\Theta}=\mathrm{diag}\left(\eta_1\mathrm{e}^{j\theta_1},\cdots,\eta_n\mathrm{e}^{j\theta_n},\cdots,\eta_N\mathrm{e}^{j\theta_N}\right)\in\mathbb{C}^{N\times N}$ is a diagonal matrix, and it is used to capture the reflective properties of the IRS. Here, the nth diagonal element, $\eta_n\mathrm{e}^{j\theta_n}$, represents the complex-valued reflection coefficient of the nth reflector of the IRS in which η_n is its magnitude while θ_n is the phase-shift. By exploiting the properties of $\mathbf{\Theta}$, we can rewrite the signal received at R as

$$y_R=\sqrt{P}\sum\nolimits_{n\in\mathcal{N}}h_n^R\eta_n\mathrm{e}^{j\theta_n}h_n^I x+w_R. \tag{4}$$

During the second time-slot, R first amplifies its received signal and then forwards it towards D [8], [16]. Thus, the signal received at D can be written as

$$\begin{aligned}y_D&=Gh^D y_R+w_D\\&=\sqrt{P}Gh^D\sum\nolimits_{n\in\mathcal{N}}h_n^R\eta_n\mathrm{e}^{j\theta_n}h_n^I x+Gh^D w_R+w_D,\end{aligned} \tag{5}$$

where $w_D\sim\mathcal{CN}\left(0,\sigma_{w_D}^2\right)$ is an AWGN at D, and G denotes the relay amplification factor, which is designed to constraint the instantaneous transmit power (P_R) at R as follows:

$$G=\sqrt{P_R\Big/\left(P\left|\sum\nolimits_{n\in\mathcal{N}}\eta_n\beta_{h_n^R}\beta_{h_n^I}\mathrm{e}^{j\phi_n}\right|^2+\sigma_{w_R}^2\right)}, \tag{6}$$

where $\phi_n=\theta_n+\theta_{h_n^R}+\theta_{h_n^I}$. By using (5), we compute the received SNR at D as

$$\gamma=\frac{P\left|Gh^D\sum_{n\in\mathcal{N}}h_n^R\eta_n\mathrm{e}^{j\theta_n}h_n^I\right|^2}{\left|Gh^D\right|^2\sigma_{w_R}^2+\sigma_{w_D}^2}. \tag{7}$$

Then, we rewrite this SNR by substituting (1) into (7) in terms of the channel phases as

$$\gamma=\frac{P\left|G\beta_{h^D}\mathrm{e}^{j\theta_{h^D}}\sum_{n\in\mathcal{N}}\eta_n\beta_{h_n^R}\beta_{h_n^I}\mathrm{e}^{j\phi_n}\right|^2}{\left|G\beta_{h^D}\mathrm{e}^{j\theta_{h^D}}\right|^2\sigma_{w_R}^2+\sigma_{w_D}^2}. \tag{8}$$

Based on (8), we maximize the received SNR at D by smartly adjusting the phase-shifts (θ_n) at each reflector to enable constructive addition of the signal terms inside the summation of the numerator of (8). To this end, the optimal choice of θ_n to maximize the received SNR at D is given by

$$\theta_n^*=\underset{-\pi\le\theta_n\le\pi}{\mathrm{argmax}}\ \gamma=-\left(\theta_{h_n^R}+\theta_{h_n^I}\right),\quad \text{for}\quad n\in\mathcal{N}. \tag{9}$$

By substituting θ_n^* into (8), the optimal SNR at D can be derived as

$$\gamma^*=\frac{P\left(G^*\right)^2\beta_{h^D}^2\left(\sum_{n\in\mathcal{N}}\eta_n\beta_{h_n^R}\beta_{h_n^I}\right)^2}{\left(G^*\right)^2\beta_{h^D}^2\sigma_{w_R}^2+\sigma_{w_D}^2} \tag{10a}$$

$$=\frac{\bar{\gamma}_R\bar{\gamma}_D\beta_{h^D}^2\left(\sum_{n\in\mathcal{N}}\eta_n\beta_{h_n^R}\beta_{h_n^I}\right)^2}{\bar{\gamma}_R\left(\sum_{n\in\mathcal{N}}\eta_n\beta_{h_n^R}\beta_{h_n^I}\right)^2+\bar{\gamma}_D\beta_{h^D}^2+1}, \tag{10b}$$

where $\bar{\gamma}_R=P_R/\sigma_{w_R}^2$ and $\bar{\gamma}_D=P/\sigma_{w_D}^2$. Moreover, in (10a), G^* is the optimal relay gain, which can be obtained by substituting θ_n^* into (6).

III. Preliminary Analysis

In this section, the optimal received SNR (10b) is probabilistically characterized by deriving a tight approximate to its CDF. First, we define $Z=\sum_{n\in\mathcal{N}}\eta_n\beta_{h_n^R}\beta_{h_n^I}$. Then, by using the fact that the envelops $\beta_{h_n^R}$ and $\beta_{h_n^I}$ are independent Rayleigh distributed random variables, Z is closely approximated by an one-sided Gaussian distributed random variable $(\tilde{Z})$ by invoking the CLT [15] as [17] (Appendix A)

$$f_Z(y)\approx f_{\tilde{Z}}(y)=\frac{\psi}{\sqrt{2\pi\sigma_Z^2}}\exp\left(\frac{-(y-\mu_Z)^2}{2\sigma_Z^2}\right),\ \text{for}\ y\ge 0. \tag{11}$$

Here, we use $\psi\triangleq 1/\mathcal{Q}\left(-\mu_Z/\sigma_Z\right)$ to normalize the PDF of Z such that $\int_{-\infty}^{\infty}f_{\tilde{Z}}(x)dx=1$, and $\mathcal{Q}(\cdot)$ denotes the Gaussian-$\mathcal{Q}$ function [15]. Moreover, μ_Z and σ_Z^2 are given by

$$\mu_Z=\sum\nolimits_{n\in\mathcal{N}}\pi\eta_n\left(\xi_{h_n^R}\xi_{h_n^I}\right)^{1/2}/2, \tag{12a}$$

$$\sigma_Z^2=\sum\nolimits_{n\in\mathcal{N}}\eta_n^2\xi_{h_n^R}\xi_{h_n^I}\left(16-\pi^2\right)/4. \tag{12b}$$

Next, we define γ_R to be

$$\gamma_R=\bar{\gamma}_R Z^2=\bar{\gamma}_R\left(\sum\nolimits_{n\in\mathcal{N}}\eta_n\beta_{h_n^R}\beta_{h_n^I}\right)^2. \tag{13}$$

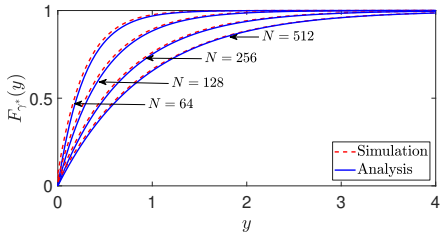

Fig. 2. The CDF of SNR (γ^*) for $N \in \{64, 128, 256, 512\}$ and $\bar{\gamma} = 10$ dB.

By using (11), PDF transformation technique can be used to evaluate a tight approximation for the PDF of γ_R as

$$f_{\gamma_R}(x) \approx \frac{\psi}{2\sqrt{\pi\sigma_R^2 x}} \exp\left(\frac{-(\sqrt{x}-\mu_R)^2}{2\sigma_R^2}\right), \text{ for } x \geq 0, \quad (14)$$

where $\mu_R = \sqrt{\bar{\gamma}_R}\mu_Z$ and $\sigma_R^2 = \bar{\gamma}_R\sigma_Z^2$. By using (14), we derive an approximated CDF for γ_R as

$$F_{\gamma_R}(x) \approx 1 - \psi\mathcal{Q}\left((\sqrt{x}-\mu_R)/\sigma_R\right), \text{ for } x \geq 0. \quad (15)$$

Next, we define γ_D to be $\gamma_D = \bar{\gamma}_D\beta_{h^D}^2$. From the PDF of β_{h^D} in (2), the CDF of γ_D is derived as

$$F_{\gamma_D}(x) = 1 - \exp\left(-x/\sigma_D^2\right), \text{ for } x \geq 0, \quad (16)$$

where $\sigma_D^2 = \bar{\gamma}_D\zeta_{h^D}$. Then, since the exact derivation of the CDF of γ^* (10b) appears to be mathematically involved, we resort to an asymptotically exact upper bound as [6]

$$\gamma^* \approx \tilde{\gamma}^* = \min\left(\bar{\gamma}_R\left(\sum\nolimits_{n\in\mathcal{N}} \eta_n\beta_{h_n^R}\beta_{h_n^I}\right)^2, \bar{\gamma}_D\beta_{h^D}^2\right). \quad (17)$$

By noticing that $\tilde{\gamma}^* = \min(\gamma_R, \gamma_D)$, we derive the approximated CDF of γ^* (or the exact CDF of $\tilde{\gamma}^*$) as [15]

$$\begin{aligned} F_{\gamma^*}(y) &\approx F_{\tilde{\gamma}^*}(y) = 1 - (1 - F_{\gamma_R}(y))(1 - F_{\gamma_D}(y)) \\ &= 1 - \psi\mathcal{Q}\left((\sqrt{y}-\mu_R)/\sigma_R\right)\exp\left(-y/\sigma_D^2\right). \end{aligned} \quad (18)$$

Next, we validate the accuracy of the approximated CDF of γ^* (18). We plot (18) and compare it with the Monte-Carlo simulations of the exact optimal SNR (10b) in Fig. 2 for various $N \in \{64, 128, 256, 512\}$. Fig. 2 illustrates that our analytical CDF approximation is accurate for medium-to-large numbers of reflective elements (N) at the IRS. A relatively larger N is practically feasible and cost effective for IRSs, and hence, our probabilistic characterization of the optimal SNR (18) is useful in deriving performance bounds for the cascaded IRS-relay channels.

IV. Performance Analysis

A. Average achievable rate

First, we can define the average achievable rate as follows:

$$\mathcal{R} = \mathbb{E}\left[\frac{1}{2}\log_2(1+\gamma^*)\right], \quad (19)$$

where the pre-log factor of $1/2$ is due to the fact that half-duplex relay mode requires two time-slots for end-to-end data transmission for the proposed system model. The exact derivation of $\mathcal{R}$ in (19) seems mathematically intractable, and hence, we again resort to a tight upper bound by invoking the Jensen's inequality as [18]

$$\mathcal{R} \leq \mathcal{R}_{ub} = \frac{1}{2}\log_2(1+\mathbb{E}[\gamma^*]) \approx \frac{1}{2}\log_2(1+\mathbb{E}[\tilde{\gamma}^*]). \quad (20)$$

Then, by evaluating the expectation term in (20), an achievable rate upper bound is computed as (Appendix B)

$$\mathcal{R}_{ub} = \frac{1}{2}\log_2\left(1 + 2\psi\sigma_D^2\mathcal{Q}\left(-\mu_R/\sigma_R\right)\right). \quad (21)$$

B. The SNR/rate outage probability

For the proposed system, the probability that the instantaneous SNR (γ) falls below a threshold SNR (γ_{th}) is referred as the SNR outage probability. Thus, we obtain an approximation to this SNR outage probability from (18) as

$$P_o = \Pr(\gamma^* \leq \gamma_{th}) \approx F_{\gamma^*}(\gamma_{th}). \quad (22)$$

The rate outage probability can also be readily obtained as

$$P_o = \Pr(\mathcal{R}' \leq \mathcal{R}_{th}) = \Pr\left(\gamma^* \leq 2^{2\mathcal{R}_{th}} - 1\right) \approx F_{\gamma^*}(2^{2\mathcal{R}_{th}} - 1), \quad (23)$$

where $\mathcal{R}' = \frac{1}{2}\log_2(1+\gamma^*)$ is the achievable rate, and $\mathcal{R}_{th}$ denotes a threshold rate.

C. The average symbol error rate (SER)

The average SER of the proposed systems is defined as the expectation of the conditional error probability ($P_{e|\gamma^*}$) over the probability distribution of γ^* [19]. Here, $P_{e|\gamma^*}$ is given for a broad range of coherent modulation schemes by $P_{e|\gamma^*} = \omega\mathcal{Q}\left(\sqrt{\vartheta\gamma^*}\right)$, where the modulation scheme determines the values of fixed parameters ω and ϑ [19]. Thereby, we can define the average SER as $\bar{P}_e = \mathbb{E}\left[\omega\mathcal{Q}\left(\sqrt{\vartheta\gamma^*}\right)\right]$. By using the CDF of γ^* in (18), a tight approximation for $\bar{P}_e$ can be given as [7]

$$\bar{P}_e \approx \frac{\omega}{2} - \frac{\omega\sqrt{\vartheta}}{2\sqrt{2\pi}}\int_0^\infty x^{-1/2}\exp\left(-\frac{\vartheta x}{2}\right)\bar{F}_{\tilde{\gamma}^*}(x)dx, \quad (24)$$

where $\bar{F}_{\tilde{\gamma}^*}(x) = 1 - F_{\tilde{\gamma}^*}(x)$ is the complementary CDF (CCDF) of γ^*. Then, the closed-form solution to $\bar{P}_e$ is given by evaluating the integration in (24) as follows (Appendix C):

$$\begin{aligned} \bar{P}_e \approx \frac{\omega}{2} + 2\lambda\mathcal{Q}\left(-\mu_R/\sigma_R\right) + \frac{\lambda}{\pi\sqrt{a\sigma_R^2}}\mathrm{e}^{\frac{-\mu_R^2}{2\sigma_R^2}\left(1-\frac{1}{2a\rho\sigma_R^2}\right)} \\ \times\sum\nolimits_{i\in C_\infty}(-2)^i\left(\frac{\sqrt{a}\rho^2\sigma_R^2}{\mu_R}\right)^{i+1}\Gamma\left(\frac{i+1}{2}, \frac{\mu_R^2}{2a\rho\sigma_R^4}\right), \end{aligned} \quad (25)$$

where $\Gamma(\alpha, x) = \int_x^\infty \mathrm{e}^{-t}t^{\alpha-1}dt$ is the upper incomplete Gamma function [20, Eqn. 8.350.2]. Moreover, a, λ, and ρ are defined as

$$a = \frac{\vartheta}{2} + \frac{1}{\sigma_D^2}, \quad \lambda = \frac{\omega\psi\sqrt{\vartheta}}{\sqrt{a}}, \quad \text{and} \quad \rho = 1 + \frac{1}{2a\sigma_R^2}. \quad (26)$$

In (25), even though there is an infinite summation, this analysis is accurate for a small number of summation terms. For instance, we evaluate this summation term only for $i \in C_2$. Fig. 5 reveals that this analytical approximation is tight even for three summation terms.

V. Effects of Phase Quantization

In order to maximize the received SNR in (8), we assume that each IRS element provides a continuous phase-shift as per (9). However, in practice, an IRS reflecting element only uses a set of discrete phase-shifts due to the associated hardware limitations. Thus, we investigate the impact of phase-shift quantization assuming that a limited number of discrete phase-shift is available for selection at the nth IRS element

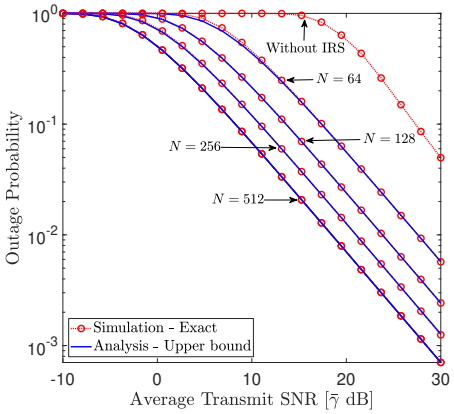

Fig. 3. The outage probability for $N \in \{64, 128, 256, 512\}$ and the threshold SNR is $\gamma_{th} = 0$ dB.

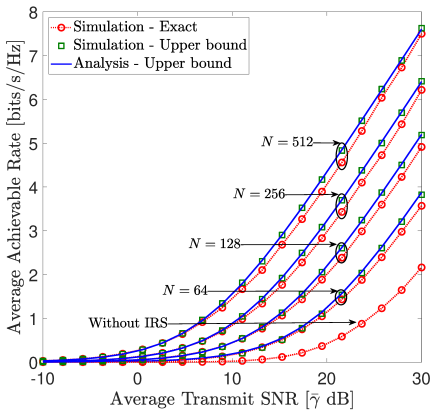

Fig. 4. The average achievable rate for $N \in \{64, 128, 256, 512\}$.

as $\hat{\theta}_n^* = \pi\hat{q}/2^{b-1}$, where b is the number of quantization bits for the discrete phase-shifts at IRS. Then, $\hat{q}$ is given by $\hat{q} = \underset{q\in\{0,\pm1,\cdots,\pm2^{b-1}\}}{\text{argmin}} |\theta_n^* - \pi q/2^{b-1}|$, and $\hat{\theta}_n^*$ is the optimal phase-shift (9). Then, the difference between unquantized and quantized phase-shift is defined as the phase quantization error: $\epsilon_n = \theta_n^* - \hat{\theta}_n^*$. When the number of quantization levels increases, ϵ_n converges to a uniform distribution as $\epsilon_n \sim \mathcal{U}[-\pi/2^b, \pi/2^b)$ [21]. Also, ϵ_n becomes uncorrelated with the signal. Thus, the optimal SNR in (10b) with discrete phase-shifts can be given as

$$\hat{\gamma}^* = \frac{\bar{\gamma}_R\bar{\gamma}_D\beta_{h^D}^2\left(\sum_{n\in\mathcal{N}}\eta_n\beta_{h_n^R}\beta_{h_n^I}\mathrm{e}^{j\epsilon_n}\right)^2}{\bar{\gamma}_R\left(\sum_{n\in\mathcal{N}}\eta_n\beta_{h_n^R}\beta_{h_n^I}\mathrm{e}^{j\epsilon_n}\right)^2 + \bar{\gamma}_D\beta_{h^D}^2 + 1}. \quad (27)$$

This optimal SNR expression (27) can be used to investigate the detrimental impact of discrete phase-shifts for the proposed system model.

VI. Numerical Results

In this section, the performance of the proposed IRS-assisted relay system is evaluated numerically. The large-scale fading is modeled by $\zeta_{ab} = (d_0/d_{ab})^\nu \times 10^{\varphi_{ab}/10}$, where d_{ab} for $\{a, b\} \in \{S, \text{IRS}, R, D\}$, $d_0 = 1$ m, and $\nu = 3.4$ are the distance between nodes a and b, the reference distance, and the path-loss exponent, respectively. Furthermore, the log-normal shadow fading is accounted by $10^{\varphi_{ab}/10}$ with $\varphi_{ab} \sim (0, 8)$ [22]. In simulations, we model the AWGN variances at R ($\sigma_{w_R}^2$) and D ($\sigma_{w_D}^2$) as $\sigma_{w_R}^2 = \sigma_{w_D}^2 = 10\log_{10}(N_0BN_f)$ dB, where $N_0 = -174$ dBm/Hz, $B = 20$ MHz is the transmission bandwidth, and $N_f = 7$ dB is the noise figure. Moreover, all the nodes (S, IRS, R, and D) are placed in fixed positions over an area of $1000 \times 2000\,\text{m}^2$. Specifically, the distances between S-IRS, IRS-R, and R-D are 550 m, 600 m, and 500 m, respectively. The amplitude of reflection coefficients η_n for $n \in \mathcal{N}$ is set to 0.9. Unless otherwise specified, the average transmit SNR is defined as $\bar{\gamma} = \bar{\gamma}_R = \bar{\gamma}_D$.

In Fig. 3, the SNR outage probability is plotted against $\bar{\gamma}$ for a distinct set of reflective elements at the IRS defined by $N \in \{64, 128, 256, 512\}$. The outage probability of S-R-D transmission (without using an IRS) is also plotted for comparison purposes. We use Monte-Carlo simulation to generate the exact outage curves for the purpose of validating the accuracy of our analytical outage probability in (22). The tightness of our outage probability approximation notably increases with N. As per Fig. 3, the outage probability performance is boosted with the number of reflective elements at the IRS. For instance, the case with $N = 64$ needs an average transmit SNR of 27.6 dB to obtain an outage probability of 10^{-2}, which is 14.2%, 22.5%, and 34.8% increase over the IRS with $N = 128$, $N = 256$, and $N = 512$ cases, respectively. Moreover, Fig. 3 illustrates that the proposed IRS-assisted relay system outperforms S-R-D transmission in terms of outage probability. For example, to attain an outage probability of 10^{-1}, S-R-D set-up requires an average transmit SNR of 27 dB, and it is about 41.2% increment in terms of average transmit SNR demand over the case with $N = 64$.

In Fig. 4, we investigate the impact of the number of IRS elements on the average achievable rate by plotting the average achievable rate as a function of $\bar{\gamma}$ for $N \in \{64, 128, 256, 512\}$. We also plot the achievable rate of the S-R-D transmission to compare with the proposed system. The analytical upper bound of the achievable rate in (21) is validated by plotting the exact rate curves via Monte-Carlo simulation. For moderately large N, Fig. 4 clearly indicates that our upper bound is tight. We observe that when a higher number of reflective elements is employed at the IRS, the average achievable rate increases. For instance, at an average transmit SNR of 15 dB, $N = 128$ case provides a rate gain of 108.3% compared to the case with $N = 64$. Furthermore, this rate gain increases to 245.6% and 425.4.0% for $N = 256$ and $N = 512$ cases, respectively. In Fig. 4, we observe that the achievable rate can be boosted by adopting IRS over conventional relay networks. For instance, a rate gain of 185.6% can be achieved by using an IRS with $N = 64$ compared to the S-R-D transmission at an average transmit SNR of 20 dB.

In Fig. 5, the average bit error rate (BER) of binary phase-shift keying (BPSK) is plotted against $\bar{\gamma}$ for $N \in \{64, 128, 256, 512\}$. The exact BER curves are generated via the Monte-Carlo simulations to validate the accuracy of our analysis, while the analytical curves are plotted via the analysis in (25) by substituting $\omega = 1$ and $\vartheta = 2$. Fig. 5 illustrates that the proposed cascaded IRS-R set-up outperforms the S-R-D

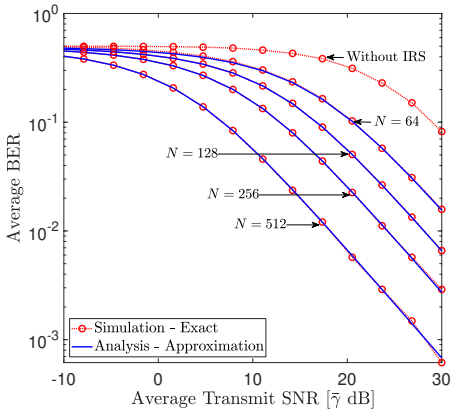

Fig. 5. The average BER of BPSK for $N \in \{64, 128, 256, 512\}$, $\omega = 1$, and $\vartheta = 2$.

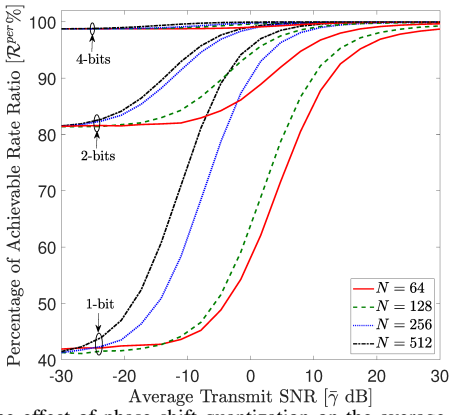

Fig. 6. The effect of phase shift quantization on the average achievable rate for $N \in \{64, 128, 256, 512\}$.

transmission in terms of the average BER. Fig. 5 also depicts that the performance of the proposed system can be boosted in terms of the average BER by increasing the number of reflective elements at the IRS. For example, to achieve an average BER of 10^{-2}, the set-up with $N = 128$ case requires an average transmit SNR of 28 dB, which is an 10.5 dB increase compared to the transmit SNR requirement of the case with $N = 512$.

In Fig. 6, the percentage rate ratio ($\mathcal{R}^{per}$) is plotted against $\bar{\gamma}$ for different $N \in \{64, 128, 256, 512\}$ to investigate the effect of phase quantization used in IRS for controlling discrete phase-shifts. The phase-shift quantization errors are randomly generated to be uniformly distributed: $\mathcal{U}[-\pi/2^b, \pi/2^b)$. The ratio between the average achievable rate with phase-shift quantization errors and the rate without phase-shift quantization errors defines the percentage rate ratio: $\mathcal{R}^{per} = \hat{\mathcal{R}}/\mathcal{R} \times 100\%$. Fig. 6 shows that the effect of phase-shift errors becomes negligible for higher values of b. Specifically, when 4-bits quantization is used at each IRS element, we can achieve more than 99% of the average rate compared to the continuous phase-shifts. Also, $\mathcal{R}^{per}$ improves with higher values for the average transmit SNR. For instance, we can achieve more than 94%, 98%, and almost 100% average rate with 1, 2, and 4-bits quantization, at transmit SNR beyond 20 dB. Fig. 6 also depicts that a higher number of IRS elements is beneficial in achieving a better average rate in the moderate-to-large SNR regime.

VII. Conclusion

The performance of an IRS-assisted relay system has been investigated. The optimal SNR that is attained through intelligent phase-shift controlling of the IRS elements has been probabilistically characterized by deriving a tight CDF approximation. Thereby, tight approximations/bounds for the fundamental performance metrics, including the average achievable rate, SNR/rate outage probability, and average SER have been derived. The impact of phase-shift errors at the IRS has been investigated by adopting discrete phase-shift adjustments. The accuracy of our analysis has been validated through the Monte-Carlo simulation. A rigorous set of numerical results has been presented to investigate the performance of the proposed IRS-assisted relay system. From our numerical results, we reveal that IRS-assisted relay systems can enhance end-to-end wireless communication performance.

Appendix A
Derivation of PDF of Z in (11)

First, we define $Z = \sum_{n\in\mathcal{N}} z_n$, where $z_n = \eta_n \beta_{h_n^R} \beta_{h_n^I}$. Since $\beta_{h_n^R}$ and $\beta_{h_n^I}$ are independently distributed Rayleigh random variables with parameters $\xi_{h_n^I}$ and $\xi_{h_n^R}$, respectively, the kth moment of z_n can be given as [23]

$$\mathbb{E}\left[z_n^k\right] = \left(\eta_n^2 \xi_{h_n^I} \xi_{h_n^R}\right)^{k/2} \left(\Gamma(k/2+1)\right)^2, \tag{28}$$

where $\Gamma(t) = \int_0^\infty x^t \mathrm{e}^{-x} dx$ is the Gamma function [20, Eqn. 8.310.1]. Then, we approximate the PDF of Z by an one sided Gaussian distribution in moderately large regime of N as $Z \sim \left(\mu_Z, \sigma_Z^2\right)$ by invoking the CLT. Here, μ_Z and σ_Z^2 are defined in (12a) and (12b), respectively. Finally, we can give the PDF of Z as (11).

Appendix B
Derivation of $\mathcal{R}_{ub}$ in (21)

The kth moment of $\tilde{\gamma}^*$ can be defined by using the CDF of $\tilde{\gamma}^*$ as follows [15]:

$$\mathbb{E}\left[(\tilde{\gamma}^*)^k\right] = \int_0^\infty k x^{k-1} \left(1 - F_{\tilde{\gamma}^*}(x)\right) dx, \text{ for } k \geq 1. \tag{29}$$

Then, by substituting the CDF of $\tilde{\gamma}^*$ in (18) into (29) and for $k = 1$, $\mathbb{E}[\tilde{\gamma}^*]$ can be calculated as

$$\begin{aligned}
\mathbb{E}[\tilde{\gamma}^*] &= \int_0^\infty \psi \mathcal{Q}\left(-(\sqrt{x} - \mu_R)/\sigma_R\right) \mathrm{e}^{-x/\sigma_D^2} dx \qquad (30)\\
&\overset{(a)}{=} 2\sigma_R \psi \int_{-\mu_R/\sigma_R}^\infty (\sigma_R u + \mu_R) \mathcal{Q}(u) \, \mathrm{e}^{-(\sigma_R u + \mu_R)^2/\sigma_D^2} du\\
&\overset{(b)}{=} \psi \sigma_D^2 \left[\mathrm{e}^{-(\sigma_R u + \mu_R)^2/\sigma_D^2} \left(\mathrm{erf}\left(u/\sqrt{2}\right) - 1\right)\right]_{-\mu_R/\sigma_R}^\infty\\
&\quad + \frac{\psi \sigma_D^2 \sqrt{2}}{\sqrt{\pi}} \int_{-\mu_R/\sigma_R}^\infty \mathrm{e}^{-(\sigma_R u + \mu_R)^2/\sigma_D^2 - u^2/2} du\\
&= 2\psi\sigma_D^2 \mathcal{Q}\left(-\mu_R/\sigma_R\right) + \frac{\psi\sigma_D^2\sqrt{2}}{\sqrt{\pi}}\\
&\quad \times \underbrace{\int_{-\mu_R/\sigma_R}^\infty \mathrm{e}^{\left(\sqrt{\frac{-\sigma_R^2}{\sigma_D^2} - \frac{1}{2}}\, u - \frac{\sigma_R \mu_R}{\sigma_D^2 \sqrt{\frac{-\sigma_R^2}{\sigma_D^2} - \frac{1}{2}}}\right)^2 - \frac{\sigma_R^2 \mu_R^2}{\sigma_D^4\left(\frac{-\sigma_R^2}{\sigma_D^2} - \frac{1}{2}\right)} - \frac{\mu_R^2}{\sigma_D^2}} du}_{I},
\end{aligned}$$

where $\mathrm{erf}(x) = 2/\sqrt{\pi} \int_0^x \mathrm{e}^{-t} dt$ is the Gauss error function [20, Eqn. 8.250.1], the step (a) is obtained by letting $u = (\sqrt{x} -$

$\mu_R)/\sigma_R$, and the step (b) is computed by using integration-by-part technique. Upon several mathematical manipulations, solution to the integral I in (30) can be given in the form of $I = A\left[\text{erfi}\left(-j\delta u\right)\right]_{-\mu_R/\sigma_R}^{\infty}$, where A, δ are constants, and $\text{erfi}\left(z\right) = \text{erf}\left(jz\right)/j$ is the imaginary error function [20]. From the properties of imaginary error function, it can be shown that the solution of I becomes zero except if $\mu_R/\sigma_R = 0$. Since $\mu_R \neq 0$ and $\sigma_R > 0$, a solution to $\mathbb{E}[\tilde{\gamma}^*]$ is given as

$$\mathbb{E}[\tilde{\gamma}^*] = 2\psi\sigma_D^2\,\mathcal{Q}\left(-\mu_R/\sigma_R\right). \tag{31}$$

By substituting (31) into (20), $\mathcal{R}_{ub}$ is derived as (21).

Appendix C
Derivation of $\bar{P}_e$ in (25)

By substituting $F_{\tilde{\gamma}^*}(y)$ into (24), the integral (I_P) in (24) can be evaluated as

$$\begin{aligned}
I_P &= \frac{2\lambda\sqrt{a}}{\sqrt{2\pi}}\int_0^{\infty} x^{-1/2}\mathrm{e}^{-ax}\mathcal{Q}\left(\frac{\sqrt{x}-\mu_R}{\sigma_R}\right)dx \qquad (32)\\
&\overset{(c)}{=} \frac{4\lambda\sigma_R\sqrt{a}}{\sqrt{2\pi}}\int_{-\mu_R/\sigma_R}^{\infty}\mathrm{e}^{-a(\sigma_R u+\mu_R)^2}\mathcal{Q}\left(u\right)du\\
&\overset{(d)}{=} \sqrt{2}\lambda\left[\mathcal{Q}\left(u\right)\text{erf}\left(\sqrt{a}(\sigma_R u+\mu_R)\right)\right]_{-\mu_R/\sigma_R}^{\infty}\\
&\quad+\frac{\lambda}{\sqrt{\pi}}\int_{-\mu_R/\sigma_R}^{\infty}\mathrm{e}^{-u^2/2}\text{erf}\left(\sqrt{a}(\sigma_R u+\mu_R)\right)du\\
&\overset{(e)}{=} \frac{\lambda}{\sqrt{\pi}}\int_{-\mu_R/\sigma_R}^{\infty}\mathrm{e}^{-u^2/2}du-\frac{\lambda}{\pi}\int_{-\mu_R/\sigma_R}^{\infty}\frac{\mathrm{e}^{-u^2/2}\mathrm{e}^{-a(\sigma_R u+\mu_R)^2}}{\sqrt{a}(\sigma_R u+\mu_R)}\\
&\overset{(f)}{=} 2\lambda\mathcal{Q}\left(-\mu_R/\sigma_R\right)-\frac{\lambda}{\pi}\underbrace{\int_{-\mu_R/\sigma_R}^{\infty}\frac{\mathrm{e}^{-u^2/2}\mathrm{e}^{-a(\sigma_R u+\mu_R)^2}}{\sqrt{a}(\sigma_R u+\mu_R)}}_{I_P'},
\end{aligned}$$

where a and λ are defined in (26). The step (c) is due to a changing of variable technique as $u = (\sqrt{x}-\mu_R)/\sigma_R$. The step (d) is evaluated via the part-by-part integration technique. The step (e) is evaluated via a tight approximation for the error function: $\text{erf}\left(x\right) = 1-\exp\left(-x^2\right)/(x\sqrt{\pi})$ [24]. In (32), the step (f) is derived by using [20, Eqn. 2.33.2]. Then, the integral I_P' in (32) can be evaluated by substituting $t = \sqrt{a}(\sigma_R u+\mu_R)$ as

$$\begin{aligned}
I_P' &= \frac{\mathrm{e}^{\frac{-\mu_R^2}{2\sigma_R^2}}}{\sqrt{a\sigma_R^2}}\int_0^{\infty}\frac{1}{t}\mathrm{e}^{-\rho t^2+\mu_R t/(\sqrt{a}\sigma_R)}dt \qquad (33)\\
&= \frac{\mathrm{e}^{\frac{-\mu_R^2}{2\sigma_R^2}\left(1-\frac{1}{2a\rho\sigma_R^2}\right)}}{\sqrt{a\sigma_R^2}}\int_0^{\infty}\frac{1}{t}\mathrm{e}^{-\rho(t-q)^2}dt\\
&\overset{(g)}{=} \frac{\mathrm{e}^{\frac{-\mu_R^2}{2\sigma_R^2}\left(1-\frac{1}{2a\rho\sigma_R^2}\right)}}{\sqrt{a\sigma_R^2}}\int_{-q}^{\infty}\frac{1}{y+q}\mathrm{e}^{-\rho y^2}dy\\
&\overset{(h)}{=} \frac{\mathrm{e}^{\frac{-\mu_R^2}{2\sigma_R^2}\left(1-\frac{1}{2a\rho\sigma_R^2}\right)}}{\sqrt{a\sigma_R^2}}\sum_{i\in C_{\infty}}(-1)^i q^{-1-i}\int_{-q}^{\infty}y^i\mathrm{e}^{-\rho y^2}dy\\
&\overset{(i)}{=} \frac{\mathrm{e}^{\frac{-\mu_R^2}{2\sigma_R^2}\left(1-\frac{1}{2a\rho\sigma_R^2}\right)}}{\sqrt{a\sigma_R^2}}\sum_{i\in C_{\infty}}\frac{(-1)^i q^{-1-i}}{2\rho^{i/2+1/2}}\Gamma\left(\frac{i+1}{2},\rho q^2\right),
\end{aligned}$$

where ρ is given in (26), and $q = \mu_R/(2\rho\sigma_R^2\sqrt{a})$. The step (g) is evaluated by letting $y = t-q$. The step (h) is obtained by expanding $(y+q)^{-1}$ via negative binomial theorem. The step (i) is due to [20, Eqn. 2.33.10]. Finally, by substituting (32) and (33) into (24), $\bar{P}_e$ can be derived as (25).

References

[1] C. Liaskos *et al.*, "A New Wireless Communication Paradigm Through Software-Controlled Metasurfaces," *IEEE Commun. Mag.*, vol. 56, no. 9, pp. 162–169, 2018.

[2] M. D. Renzo *et al.*, "Smart Radio Environments Empowered by Reconfigurable AI Meta-Surfaces: An idea whose time has come," *EURASIP J. Wireless Commun. Net.*, May 2019.

[3] H. Yang *et al.*, "A Programmable Metasurface with Dynamic Polarization, Scattering and Focusing Control," *Scientific Reports*, vol. 6, 2016.

[4] J. Su *et al.*, "Ultrawideband, Wide Angle and Polarization-in-Sensitive Specular Reflection Reduction by Metasurface Based on Parameter-Adjustable Meta-Atoms," *Scientific Reports*, vol. 7, 2017.

[5] D. L. Galappaththige, D. Kudathanthirige, and G. Amarasuriya Aruma Baduge, "Performance Analysis of Distributed Intelligent Reflective Surface Aided Communications," in *IEEE Global Commun. Conf. (GLOBECOM)*, May 2020, pp. 1–6, (Accepted).

[6] G. Amarasuriya, C. Tellambura, and M. Ardakani, "Asymptotically-Exact Performance Bounds of AF Multi-Hop Relaying over Nakagami Fading," *IEEE Trans. Commun.*, vol. 59, no. 4, pp. 962–967, 2011.

[7] ——, "Performance Analysis Framework for Transmit Antenna Selection Strategies of Cooperative MIMO AF Relay Networks," *IEEE Trans. Veh. Technol.*, vol. 60, no. 7, pp. 3030–3044, 2011.

[8] D. Kudathanthirige, S. Timilsina, and G. A. Aruma Baduge, "Secure Communication in Relay-Assisted Massive MIMO Downlink with Active Pilot Attacks," *IEEE Trans. Inf. Forensics Security*, vol. 14, no. 11, pp. 2819–2833, 2019.

[9] C. Huang *et al.*, "Reconfigurable Intelligent Surfaces for Energy Efficiency in Wireless Communication," *IEEE Trans. Wireless Commun.*, vol. 18, no. 8, pp. 4157–4170, 2019.

[10] E. Björnson, Ö. Özdogan, and E. G. Larsson, "Intelligent Reflecting Surface Versus Decode-and-Forward: How Large Surfaces are Needed to Beat Relaying?" *IEEE Wireless Commun. Lett.*, vol. 9, no. 2, pp. 244–248, 2020.

[11] M. Di Renzo *et al.*, "Reconfigurable Intelligent Surfaces vs. Relaying: Differences, Similarities, and Performance Comparison," *IEEE Open J. Commun. Society*, vol. 1, pp. 798–807, 2020.

[12] A. A. Boulogeorgos and A. Alexiou, "Performance Analysis of Reconfigurable Intelligent Surface-Assisted Wireless Systems and Comparison With Relaying," *IEEE Access*, vol. 8, pp. 94 463–94 483, 2020.

[13] Z. Abdullah *et al.*, "Optimization of Intelligent Reflecting Surface Assisted Full-Duplex Relay Networks," *IEEE Wireless Commun. Lett.*, vol. 10, no. 2, pp. 363–367, 2021.

[14] ——, "A Hybrid Relay and Intelligent Reflecting Surface Network and Its Ergodic Performance Analysis," *IEEE Wireless Commun. Lett.*, vol. 9, no. 10, pp. 1653–1657, 2020.

[15] A. Papoulis and S. U. Pillai, *Probability, Random Variables, and Stochastic Processes*, 4th ed. McGraw Hill, 2002.

[16] G. Amarasuriya, C. Tellambura, and M. Ardakani, "Performance Analysis of Zero-Forcing for Two-Way MIMO AF Relay Networks," *IEEE Wireless Commun. Lett.*, vol. 1, no. 2, pp. 53–56, 2012.

[17] D. Kudathanthirige, D. Gunasinghe, and G. Amarasuriya, "Performance Analysis of Intelligent Reflective Surfaces for Wireless Communication," in *IEEE Int. Conf. on Commun. (ICC)*, 2020, pp. 1–6.

[18] Q. Zhang *et al.*, "Power Scaling of Uplink Massive MIMO Systems with Arbitrary-Rank Channel Means," *IEEE J. Sel. Areas Signal Process.*, vol. 8, no. 5, pp. 966–981, Oct. 2014.

[19] J. Proakis, *Digital Communications*, 4th ed. New York:McGraw-Hill, Inc., 2001.

[20] I. Gradshteyn and I. Ryzhik, *Table of Integrals, Series, and Products*, 7th ed. Academic Press, 2007.

[21] S. Haykin and M. Moher, *Communication Systems*, 5th ed. Wiley India Pvt. Limited, 2009.

[22] T. L. Marzetta *et al.*, *Fundamentals of Massive MIMO*. Cambridge University Press, Cambridge, UK, 2016.

[23] J. Salo, H. El-Sallabi, and P. Vainikainen, "The Distribution of the Product of Independent Rayleigh Random Variables," *IEEE Trans. Antennas Propag.*, vol. 54, no. 2, pp. 639–643, 2006.

[24] R. M. Howard, "Arbitrarily Accurate Analytical Approximations for the Error Function," *arXiv e-prints*, 2020.